Linking plankton size spectra and community composition to carbon export and its efficiency

Serra-Pompei, Camila; Ward, Ben A.; Pinti, Jérôme; Visser, André W.; Kiørboe, Thomas; Andersen, Ken H.

Published in:
Global Biogeochemical Cycles

Link to article, DOI:
10.1029/2021GB007275

Publication date:
2022

Document Version
Publisher's PDF, also known as Version of record

Global Biogeochemical Cycles®

AGU ADVANCING EARTH AND SPACE SCIENCE

RESEARCH ARTICLE
10.1029/2021GB007275

Linking Plankton Size Spectra and Community Composition to Carbon Export and Its Efficiency

Camila Serra-Pompei[1,2], Ben A. Ward[3], Jérôme Pinti[1,4], André W. Visser[1], Thomas Kiørboe[1], and Ken H. Andersen[1]

[1]Centre for Ocean Life, Technical University of Denmark, DTU Aqua, Kongens Lyngby, Denmark, [2]Department of Earth, Atmospheric and Planetary Sciences, Massachusetts Institute of Technology, Cambridge, MA, USA, [3]Ocean and Earth Science, University of Southampton, Southampton, UK, [4]College of Earth, Ocean and Environment, University of Delaware, Lewes, DE, USA

Key Points:

- We use a global mechanistic size-spectrum model to investigate the relation between particulate export and plankton community metrics
- We find a good correlation between export efficiency and the exponent of the size spectrum
- Total carbon export correlated well with copepod biomass and trophic level of active copepods in the model

Supporting Information:

Supporting Information may be found in the online version of this article.

Correspondence to:

C. Serra-Pompei,
camsp@mit.edu

Citation:

Serra-Pompei, C., Ward, B. A., Pinti, J., Visser, A. W., Kiørboe, T., & Andersen, K. H. (2022). Linking plankton size spectra and community composition to carbon export and its efficiency. *Global Biogeochemical Cycles*, *36*, e2021GB007275. https://doi.org/10.1029/2021GB007275

Received 13 DEC 2021
Accepted 19 APR 2022

Author Contributions:

Conceptualization: Camila Serra-Pompei, Jérôme Pinti, André W. Visser, Thomas Kiørboe, Ken H. Andersen
Data curation: Camila Serra-Pompei
Formal analysis: Camila Serra-Pompei, Ken H. Andersen
Funding acquisition: André W. Visser, Thomas Kiørboe, Ken H. Andersen
Investigation: Camila Serra-Pompei, Ben A. Ward, Jérôme Pinti, André W. Visser, Thomas Kiørboe
Methodology: Camila Serra-Pompei, Ben A. Ward, Jérôme Pinti, André W. Visser, Thomas Kiørboe, Ken H. Andersen

Abstract The magnitude and efficiency of particulate carbon export from the ocean surface depends not only on net primary production (NPP) but also on how carbon is consumed, respired, and repackaged by organisms. We contend that several of these processes can be captured by the size spectrum of the plankton community. However, most global models have relatively simple food-web structures that are unable to generate plankton size spectra. Moreover, the life-cycles of multicellular zooplankton are typically not resolved, restricting the ability of models to represent time-lags that are known to impact carbon export and its efficiency (pe-ratio). Here, we use a global mechanistic size-spectrum model of the marine plankton community to investigate how particulate export and pe-ratio relate to the community size spectrum, community composition, and time-lags between predators and prey. The model generates emergent food-webs with associated size distributions for organisms and detrital particles. To resolve time-lags between phytoplankton and zooplankton, we implement the life-cycle of multicellular zooplankton (here represented by copepods). We find that carbon export correlates best with copepod biomass and trophic level, whereas the pe-ratio correlates best with the exponent of the size spectrum and sea surface temperature (SST). Community metrics performed better than NPP or SST for both deep export and pe-ratio. Time-lags between phytoplankton and copepods did not strongly affect export or pe-ratio. We conclude by discussing how can we reconcile size spectrum theory with field sampling.

Plain Language Summary Plankton are tiny but extremely abundant aquatic organisms. Plankton lock CO_2 away from the atmosphere as they sink to the deep ocean, where carbon can be stored for hundreds of years. However, how much carbon is locked away and for how long depends on how organisms eat, defecate, and respire. We argue that these processes are reflected in the size composition of the plankton community. The size composition shows a clear relationship between the number of organisms and their body-size. The steepness of this "size-abundance relationship" describes the balance between small versus large organisms, and has been argued to reflect how energy is transferred from small to large organisms. Since large organisms create fast-sinking particles, the size-abundance relationship could be used to estimate how much carbon is being stored in the deep ocean. Here we use a computer simulation of the global plankton community to investigate how the removal of carbon relates to the plankton community and the steepness of the size-abundance relationship. We found that the size-abundance relationship, together with the quantity of large zooplankton better explained carbon export than other measures typically used, such as photosynthesis and temperature.

1. Introduction

Plankton contribute to the removal of atmospheric CO_2 by photosynthesizing in the surface ocean and sinking into the deep ocean, where remineralized carbon may remain sequestered for hundreds of years (Ducklow et al., 2001; Longhurst & Harrison, 1989). The amount of carbon exported and carbon export efficiency (the fraction of net primary production (NPP) being exported at) emerge from intricate processes that result in either carbon being respired in the surface ocean – and therefore not sequestered – or exported and respired in the deep ocean. Where and how much carbon is respired depends on the community composition and interactions between organisms who eat, respire, and excrete this carbon several times as energy flows across the food-web. However, due to the large amount of players and processes that alter carbon export, global estimates of the flux

Software: Ben A. Ward, Ken H. Andersen
Supervision: Ben A. Ward, André W. Visser, Thomas Kiørboe, Ken H. Andersen
Validation: Camila Serra-Pompei, Jérôme Pinti, André W. Visser, Thomas Kiørboe, Ken H. Andersen
Visualization: Camila Serra-Pompei
Writing – original draft: Camila Serra-Pompei, Ben A. Ward, Jérôme Pinti, André W. Visser, Thomas Kiørboe, Ken H. Andersen
Writing – review & editing: Camila Serra-Pompei, Ben A. Ward, Jérôme Pinti, André W. Visser, Thomas Kiørboe, Ken H. Andersen

out of the euphotic zone are highly uncertain, ranging from ≈3 to 12 PgC year^{-1} (DeVries & Weber, 2017; Dunne et al., 2005; Henson et al., 2011).

Community composition and interactions between organisms drive carbon export and its efficiency (Ducklow et al., 2001; Henson et al., 2019). In general, food-webs that are dominated by large organisms are expected to efficiently export large amounts of carbon (Stamieszkin et al., 2015; Wassmann, 1997). This is because large organisms produce fast-sinking particles (Small et al., 1979). These food-webs tend to be short, where NPP efficiently reaches large organisms (Wassmann, 1997). Conversely, food-webs dominated by small organisms tend to be long, with many trophic transfers. Each trophic transfer results in respiration losses, and therefore, long food-webs with many trophic levels result in carbon being exported inefficiently (Wassmann, 1997).

Time-lags between phytoplankton and zooplankton are another factor that has been suggested to affect carbon export (Henson et al., 2015, 2019; Parsons, 1988). These time-lags result from the slower demographic response of multicellular zooplankton (e.g., copepods) relative to phytoplankton growth rate. Multicellular zooplankton need to grow in body size before being able to reproduce. This ontogenetic growth prevents multicellular zooplankton populations to grow as fast as phytoplankton that grow by cell division. In contrast, unicellular zooplankton (that also grow by cell division) are able to tightly follow phytoplankton dynamics. Grazing by unicellular zooplankton often results in low export efficiencies, as they contribute to long food-webs dominated by small organisms (McNair et al., 2021), where most carbon is respired in the surface ocean. Hence, differences in life-history strategies between prey and predators can alter the amount of carbon exported.

Food-web structure, organismal size distributions, and the life cycle of organisms are therefore important factors contributing to carbon export and its efficiency. However, most models that simulate carbon export have similar simple food-web configurations. These food-web configurations often resolve a small and a large group of each component of the ecosystem: phytoplankton, zooplankton, and detritus (e.g., Bisson et al., 2020; DeVries & Weber, 2017; Henson et al., 2015; Laws et al., 2000; Siegel et al., 2014). These food-webs have fixed interactions, where the small/large zooplankton eats the small/large phytoplankton (and perhaps the large zooplankton also eats the small zooplankton). Yet, marine systems form size spectra with complex interactions (Hartvig et al., 2011; Sprules & Barth, 2016; Sprules & Munawar, 1986). Organisms of the same size can occupy different trophic levels, or the same organism can be at a different trophic level depending on the environmental conditions. In addition, in these models, no life cycle differences are made between zooplankton groups, preventing time-lags between prey and predators. Simple food-web configurations are convenient to understand some of the main interactions, but also miss several of the factors mentioned above. Hence, incorporating flexible food-web configurations, life-histories, and size spectra in ecosystem models might help identify new processes driving carbon export and its efficiency.

A major factor shaping marine food-webs is body-size (Andersen et al., 2016; Hartvig et al., 2011). Predator-prey interactions are size-dependent, where typically large eats small, and metabolic processes follow allometric relationships (Kiørboe & Hirst, 2014). In marine systems, the combination of these processes results in body-mass normalized size-spectra closely resembling power-law functions ($B = \kappa m^{\lambda}$), with varying coefficient (κ) and a negative exponent (λ) (Andersen, 2019; Sprules & Barth, 2016). Differences in the coefficient indicate differences in the bulk biomass, whereas differences in the exponent show changes in the balance of small versus large organisms, reflecting how efficiently energy and biomass reach larger organisms (Andersen et al., 2009). Among the emergent size spectra, low exponents (steeper spectra) indicate that energy is inefficiently channeled toward large organisms (inefficient food-webs), while communities with high exponents (flatter spectra) efficiently channel NPP to large organisms (efficient food-webs). The exponent of the size spectrum is thus a good indicator of food-web efficiency, and is therefore a potentially good indicator of carbon export and its efficiency.

Here we seek to understand how carbon export and its efficiency relate to community composition, food-web structure, size spectra, and trophic interactions between prey and predators. To do so, we use a mechanistic model of the planktonic community coupled to a 3D representation of a global ocean circulation model. We use the Nutrient-Unicellular-Multicellular (NUM) size-spectrum model of the planktonic community (Serra-Pompei et al., 2020). This framework is built upon the main processes at the individual level: physiology and prey size preference and encounter. The life cycle of multicellular zooplankton is also resolved, differentiating them from unicellular zooplankton. The model yields size spectra of plankton and detrital particles, which are important to

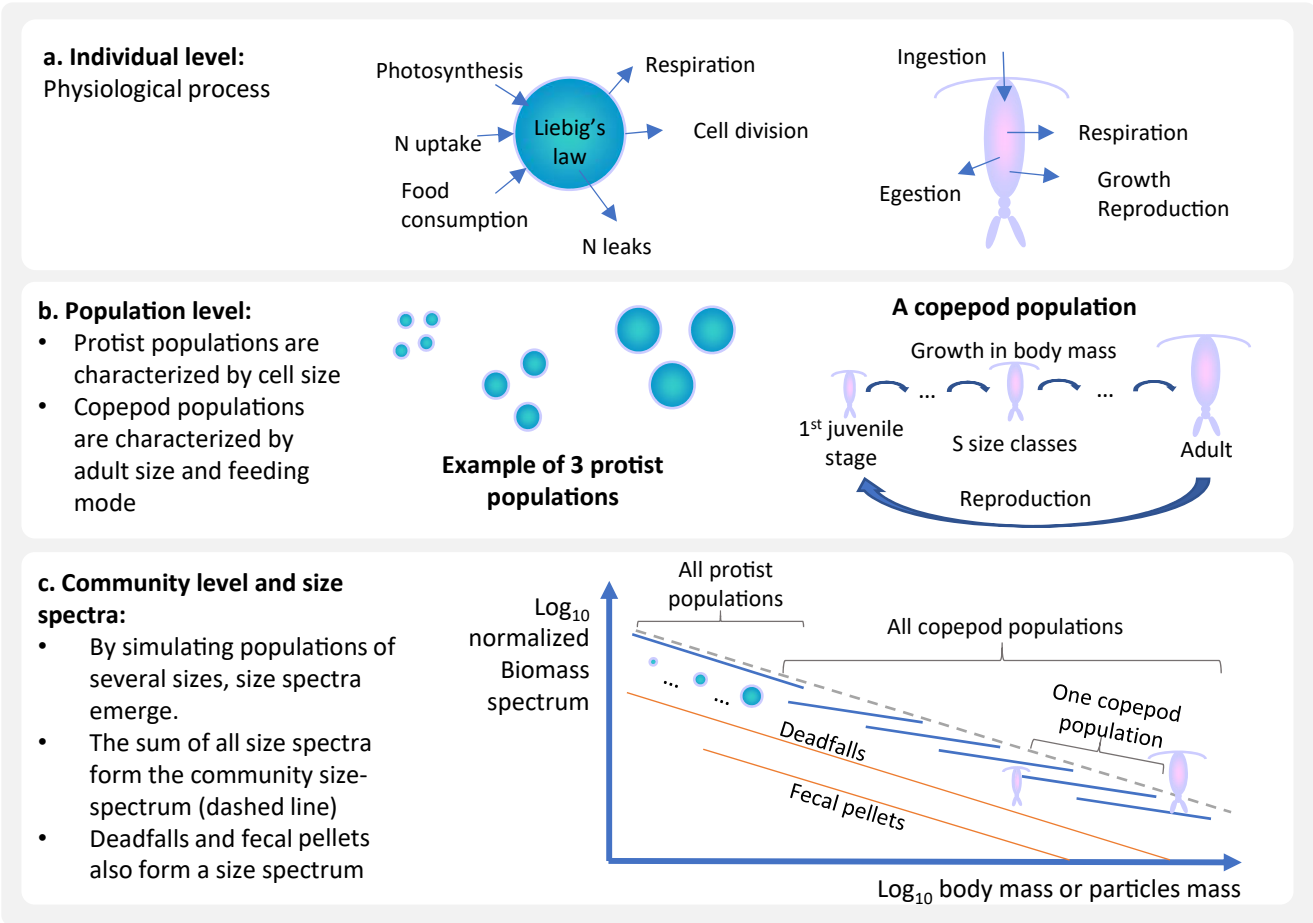

Figure 1. Diagram of the ecological model. (a) Community level processes are scaled from rates at the individual level, which depend on resources and prey availability as well as temperature and organism size. (b) A population is the combination of organisms that have the same trait combinations, here cell mass for protists and adult body mass and feeding mode (active vs. passive) for copepods (b). Finally, (c) the combination of all populations results in community-level processes and the emergence of size spectra.

determine particle sinking rates. Overall, food-web structure and the resulting particle export are emergent properties from biological interactions between organisms and the environment.

2. Methods

The NUM framework is a mechanistic size- and trait-based model of the planktonic community (Serra-Pompei et al., 2020). The original model resolves the size distribution of unicellular protists (autotrophic, mixotrophic, heterotrophic), the copepod community, copepod fecal pellets, and one pool of nitrogen. Here, the model has been extended to account for the size-distribution of dead cells and dead copepods, together referred to as deadfalls. The ecological model is embedded in a 3D transport matrix that represents advection and mixing of the ocean physical environment (Khatiwala, 2007). Here, we briefly explain the model and illustrate the main concepts (Figure 1). A detailed explanation of the model and its equations can be found in the Supporting Information S1 and in Serra-Pompei et al. (2020).

2.1. Ecological Model

The model is mechanistic, where we use empirically demonstrated mechanisms at the individual level to scale to the population, community and ecosystem levels. The model generates a community of protists, copepods, fecal pellets, and deadfalls (Figure 1c). To obtain the community size-spectrum, the model simulates several size-classes of each compartment (Figure 1b). Protists are discretized in populations characterized by the organism's

size. Copepods also have several populations, each characterized by the adult body-mass and feeding mode. Each copepod population grows in body-size as they mature from nauplii to adults that can reproduce (Figure 1b). The growth from nauplii to adulthood results in changes of up to two orders of magnitude in body mass. Copepods produce fecal pellets that are proportional to the organism size. Finally, both protists that die through viral lysis and copepods that die through non-consumptive mortality result in deadfalls of sizes that depend on the size of the producer. Therefore, size is the main trait describing organisms and particles, where physiological rates, predator-prey interactions, and sinking rates of particles are all size-dependent.

We consider different protist trophic strategies and copepod feeding modes. Here, protists are mixotrophic "generalists" (Figure 1a); that is, they can simultaneously photosynthesize, take up dissolved nutrients, and eat other organisms. Size resolves the emergence of the distinct trophic strategies across the protist size spectrum (Chakraborty et al., 2017). For example, since the smallest protists don't have prey to eat and have a competitive advantage in nitrogen uptake, they will mainly be autotrophs. On the other hand, there is more prey available for large protists, and therefore they will tend to be heterotrophs. Intermediate sized protists will tend to be mixotrophs. Still, environmemtal conditions and prey availability will define the best trophic strategy for each size-class. As for copepods, we make a distinction between "active" and "passive" feeding modes. Active copepods include cruising copepods and feeding-current feeders that encompass most calanoid copepods. Passive feeding copepods are ambush "sit-and-wait" feeders that include some calanoids and most cyclopoids. Active feeding copepods constantly search for food, have high metabolic expenditures, and are more easily detected by predators. Conversely, passive feeders avoid predation by waiting for their prey to come, resulting in a lower availability of prey. These two feeding modes include the feeding strategies of most pelagic copepods.

Organisms in the model interact through competition and predation. Copepods feed on protists, on other copepods, and on deadfalls and fecal pellets. Protists feed on other protists, but also have the ability to photosynthesise and take up dissolved nitrogen. Food that is not assimilated by copepods is egested as fecal pellets. The dead cells/bodies of organisms that die through viral lysis or other background mortality enter the deadfalls compartment. Deadfalls are remineralized and can be eaten by copepods. Overall, rather than being prescribed, the food-web configuration and resulting community trait-composition emerge from the environmental forcing (nitrogen, light, temperature), and the interactions of competition and predation.

The sinking rate of fecal pellets and deadfalls is assumed to be size-dependent (Figure D4 in the Supporting Information S1). The sinking rates of fecal pellets in the model are derived from the data in Small et al. (1979), and range from 1.5 to about 631 m d^{-1}. With regard to deadfalls, we assume a sinking rate that is weakly dependent on particle size (ranging between 2.2 and 240 m d^{-1}), consistent with observations (Alldredge & Gotschalk, 1988; Bach et al., 2019). A more detailed explanation on the derivation of sinking rates is provided in Section A.9 in the Supporting Information S1.

2.2. Biomass Spectrum

From the biomass in each size-class we obtain a size distribution of the biomass. The normalized biomass spectrum results from dividing the biomass in each size range by the size-range itself. For example, the size spectrum of protists is $P_{k,\mathrm{spec}} = P_k/\Delta_P$, and thus the unit of the biomass spectrum becomes mgC m^{-3} μgC^{-1} (where mgC m^{-3} corresponds to the biomass concentration in the water and μgC^{-1} to the bin width of the body-size range). The community size spectrum is the sum of all the size spectra. This normalization allows comparison between compartments, even when bin-sizes differ (see Sprules & Barth, 2016 and chapter two of Andersen, 2019 for more explanations regarding size spectra conversions).

2.3. Ocean Circulation and Environmental Forcing

The NUM framework is embedded within a representation of the global ocean circulation, using the "transport matrix method" (Khatiwala, 2007; Khatiwala et al., 2005). The transport matrix is derived from a coarse resolution (2.8° × 2.8°, 15 vertical levels), monthly averaged simulation of the MITgcm (http://kelvin.earth.ox.ac.uk/spk/Research/TMM/TransportMatrixConfigs, as used in Dutkiewicz et al., 2005). The coarse resolution results in the euphotic zone being resolved in only two or three layers of the transport matrix. The temperature forcing is monthly averaged. Irradiance at the ocean surface was taken from http://sites.science.oregonstate.edu/ocean.productivity/index.php. The data was afterward interpolated to fit the grid of the transport matrix.

2.4. Carbon Export and Carbon Export Efficiency (Pe-Ratio)

The particulate export efficiency (pe-ratio) is defined as the fraction of depth-integrated NPP exported as sinking particles at a given depth horizon. For both carbon export and pe-ratio, the depth horizons used in this study are 120 and 1,080 m, which are the bottom of the second and the seventh layer of the transport matrix, respectively. We consider the annual and seasonal pe-ratio. The annual pe-ratio is the ratio between NPP and export flux, both integrated over a year. The seasonal pe-ratio is the daily particle flux divided by the two weeks averaged NPP prior to export.

2.5. Numerics

The model configuration is flexible and any reasonable number of state variables can be implemented. Here, we use 14 protists size-classes (ranging from 10^{-7} μgC to $10^{-1.5}$ μgC per cell), and 8 copepod populations (6 populations of active feeding copepods and 2 populations of passive feeding copepods). Copepods range from 4×10^{-3} μgC for the smallest nauplii to 10^{4} μgC for the largest adult copepod. Each copepod population is divided into 5 size-classes going from nauplii to adults. There are 8 size classes of fecal pellets and 8 size-classes of deadfalls. There is one pool of dissolved nitrogen. The model was implemented in MATLAB and run for 30 years. In this run-time, the internal nutrient dynamics does not reach equilibrium. This would need much longer, unaffordable run times. To compensate for this, we initiate the nitrogen concentration with nitrate data from the World Ocean Atlas. By the end of the simulation, model compartments reach equilibrium, yet a small drift is present due to the internal nutrient dynamics. The code can be found in the following GitHub repository https://github.com/cam-sp/NUMmodel_global.git.

2.6. Model Testing

Outputs of the model are compared with field data extracted from the literature. Protists biomass is compared with nano- and microplankton data from the upper 50 m of the water column from three Atlantic Meridional Transects (AMT 12–14, San Martin et al., 2006). Copepod biomass is compared with data from the AMT 13 transect (López & Anadón, 2008). López and Anadón (2008) used a small mesh size and therefore included the smaller size range, which is often omitted in other studies. To calculate the copepod biomass we multiplied the average copepod body-mass by the abundance within each size-range of the study. Exponents of the size spectrum can also be found in San Martin et al. (2006), where they fitted a size spectrum to nano- and micro-plankton together with mesozooplankton data.

To compare NPP we use the data set collected in Saba et al. (2011), where NPP field data were collected from different campaigns. We show the root mean square difference (RMSD) of NPP for each region to compare with the values obtained in Saba et al. (2011):

$$RMSD = \left(\frac{1}{N} \sum_{i=1}^{N} \left[\log_{10}(NPP_m) - \log_{10}(NPP_d) \right]^2 \right)^{1/2},$$

where N is the number of data points, NPP_m the modeled NPP, and NPP_d the data values.

For particle export, we use two data-sets. First, we use the data compiled in Le Moigne et al. (2013) and extended in Henson et al. (2019), where particle export is estimated between 50 and 200 m depth with the ^{234}Th technique (Buesseler et al., 1992). The second data set is the one compiled in Lutz et al. (2007), where carbon export is estimated by using sediment traps deployed for several months at depths ranging 300–6,000 m. Data points of export that fell within the same bin and day of the transport matrix were averaged. The same procedure was done for the NPP data. Finally, we do not compare modeled pe-ratios with the ones derived in other studies. In other studies pe-ratios are often obtained by using NPP models (from remote sensing) and differences might emerge due to model differences. We therefore stick to validate NPP and export separately without checking pe-ratios from other studies.

Finally, we performed a sensitivity analysis of the model output. Due to the large run time of the model, the sensitivity analysis was scaled back from the entire global ocean to a number of individual water columns. A more detailed explanation and results can be found in section E of the Supporting Information.

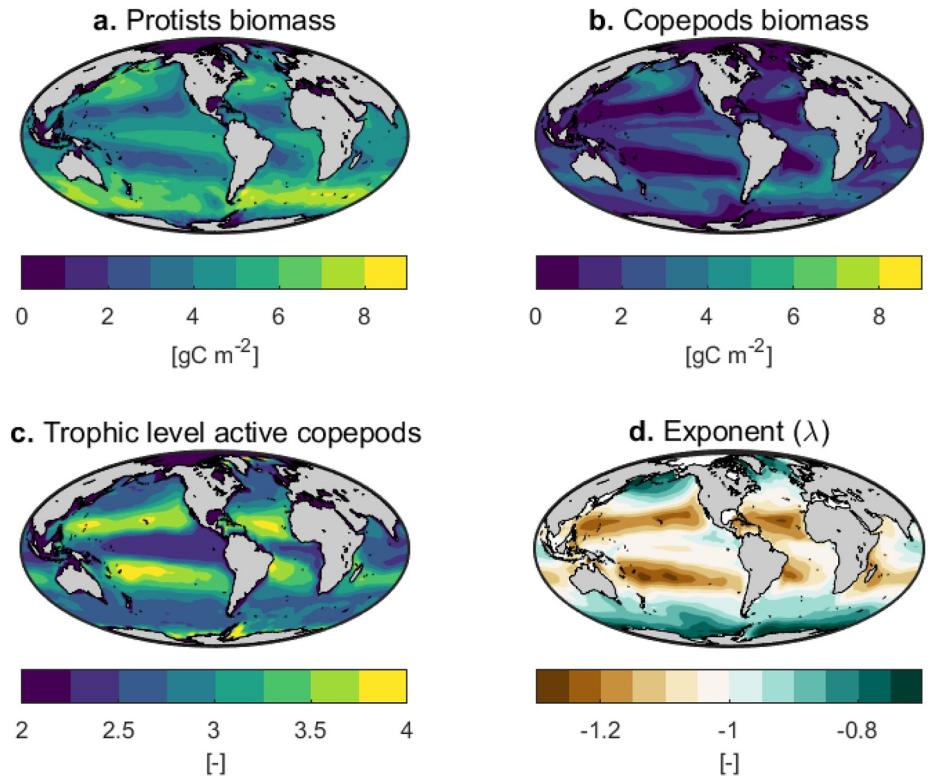

Figure 2. Model predictions: yearly averaged biomass of (a) protists and (b) copepods. (c) Average trophic level of active copepods averaged over the year (trophic level is calculated as explained in the Supporting Information S1 section B). (d) Yearly averaged exponent of the community size spectrum (see Figure D.1 in the Supporting Information S1 explaining how we fit the size spectrum and obtain the parameters).

3. Results

We start by describing the general trends of biomass and energy fluxes in the food-web while comparing them with data. Next, we investigate the drivers of food-web configurations and associated particle export and pe-ratio. All the fluxes discussed are yearly integrated, except in the last section (3.6) where we consider seasonality.

3.1. Biomass

Protist and copepod biomass follow the same global trend (Figure 2): high in temperate and sub-polar regions, and lowest in oligotrophic gyres. Compared with latitudinal field-data of nano- and microplankon biomass (Figure 3), the model falls within observed biomass ranges in the AMT 12 transect (Figure 3a), and in the northern hemisphere of the AMT 13 transect (Figure 3b). However, in the latter transect, the model overestimates biomass in the southern hemisphere. This overestimation is probably due to the lack of iron limitation in the model. The model also overestimates protist biomass in the AMT 14 transect despite following well the trend (Figure 3c). However, the biomass data from this transect is much lower than in the other two transects. Overall, despite the overestimation in some regions, modeled protist biomass follows the general trend and magnitude of the data.

Modeled copepod biomass also follows the observed trend in the AMT transect (Figure 4), despite an overestimation between latitudes −30 and −10 (stations 22 to 18). The latter follow the protist biomass trend that was also overestimated in those regions during October. Relative copepod biomass within body-size ranges is somewhat constant across latitudes, with a dominance of small copepods in most regions (Figure 4). The model simulates more small copepods than observed. Nevertheless, large copepods are present in most regions, including low productive regions, both in the data and the model.

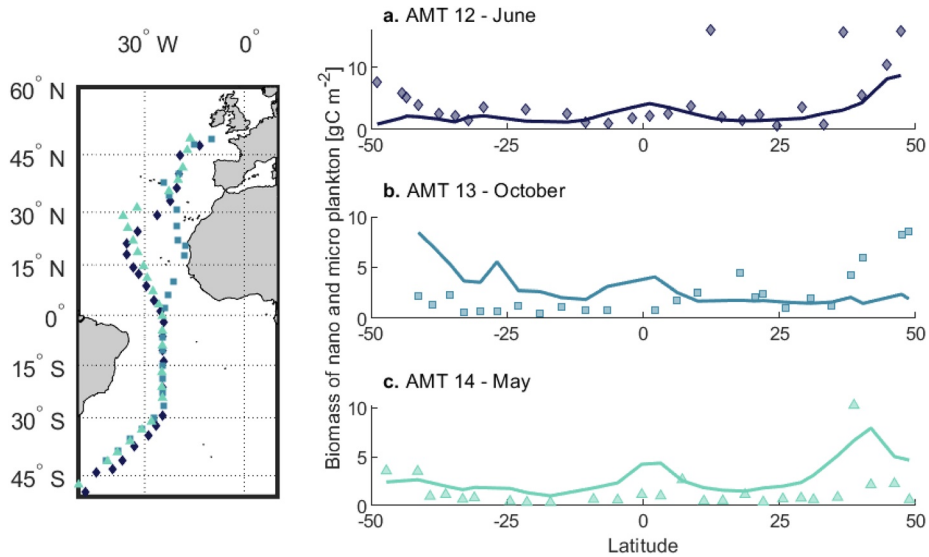

Figure 3. Nano- and micro-plankton biomass from the model (continuous lines) versus data (markers), both integrated over the upper 50 m. Biomass data is from three Atlantic Meridional Transects (AMT): (a) AMT 12 (May-June 2003), (b) AMT 13 (September-October 2003), and (c) AMT 14 (April-June 2004). Left panel shows stations where the data was collected. Data extracted from San Martin et al. (2006).

3.2. Size Spectrum

The model produces a community size spectrum (Figures 2d, 5 and 6). We fitted a power-law function ($B_{sp} = \kappa m^{\lambda}$) to the normalized community biomass spectrum to obtain the coefficient (κ) and the exponent (λ). The yearly averaged exponent varies between −1.3 and −0.7 (Figure 2d). The exponent is always negative and always close to the theoretical value of −1 (Andersen & Beyer, 2006). The lowest values (steeper slopes) appear in oligotrophic regions, and the largest values in productive regions (Figure 2). Exponents obtained from field data are also close to −1 (Figure 5). Our model fits well data trends of the AMT 12 transect and at higher latitudes of the other two transects, but underestimates the slope at low latitudes in these latter transects (Figure 5). In contrast to our model, the data yields lower exponents at higher latitudes, particularly during the spring-summer cruises (AMT 12 and 14, Figures 5a and 5c). On the other hand, our model has higher exponents at high latitudes,

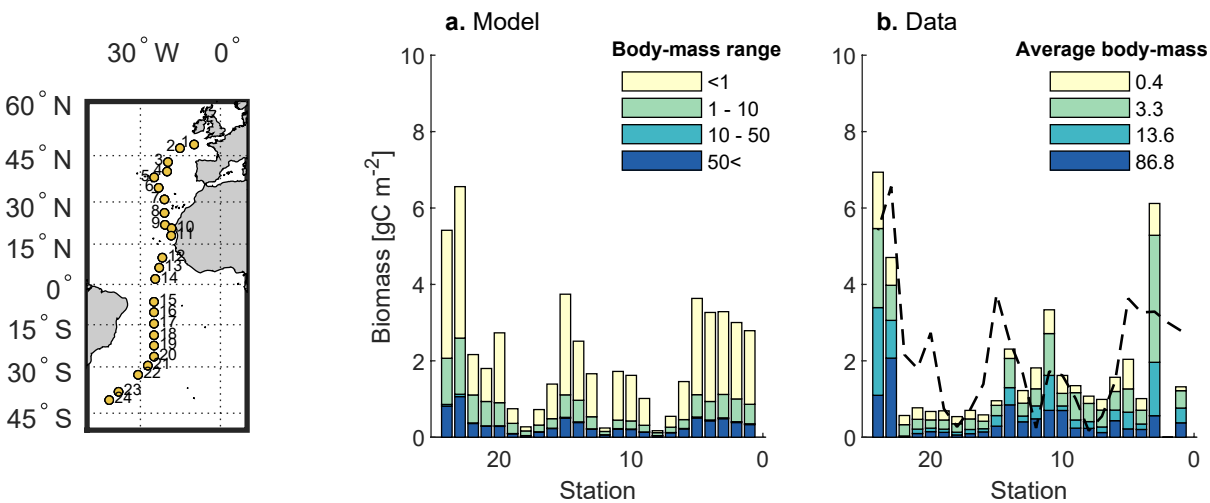

Figure 4. Copepod biomass along the Atlantic Meridional Transect for different body-size ranges (September-October). (a) Model estimates. (b) Data from López and Anadón (2008), obtained by multiplying the abundance by the average body-mass within each size range provided in their study. The smallest size-class combines adult copepods and nauplii. For easier comparison between simulated and observed data, the dashed line in panel b is the total copepod biomass from the model (from panel a). Left panel shows the stations where the data was collected in López and Anadón (2008).

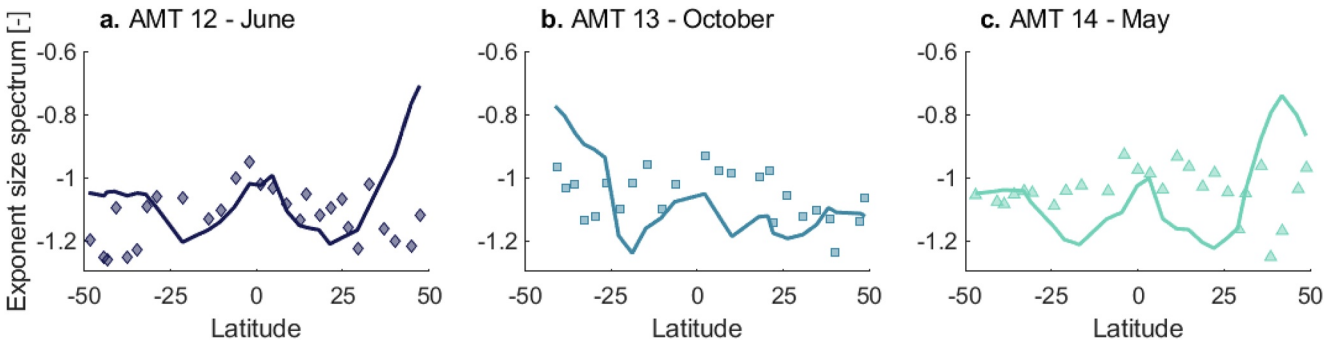

Figure 5. Exponent of the size spectrum from the model (continuous lines) and from field samples (markers). Data is from three Atlantic Meridional Transects (AMT): (a) AMT 12 (May-June 2003), (b) AMT 13 (September-October 2003), and (c) AMT 14 (April-June 2004), extracted from San Martin et al. (2006). Stations can be found in Figure 3 of this paper.

which would make sense as these systems are more productive, and therefore a "flatter" spectrum is expected. A possible reason for this discrepancy is the presence of copepods that perform seasonal migrations, which we do not have in the model. In this case, these copepods would be present earlier in the year and decrease the biomass of protists via grazing. In any case, both the data and model show an exponent always close to the theoretical prediction of -1.

Changes in the exponent seem to be driven by the presence/absence of the smallest protists size-classes and the largest copepods (Figure 6). Some parts of the size spectrum, however, do not fit well a power-law function (Figures 6b and 6c), particularly within the protists size-range (Figures D1, D2 and D3 in the Supporting Information S1). This is due to a plankton bloom, where a specific phytoplankton size group dominates the system. This highlights that a wide range of body-sizes is needed to properly fit a size spectrum.

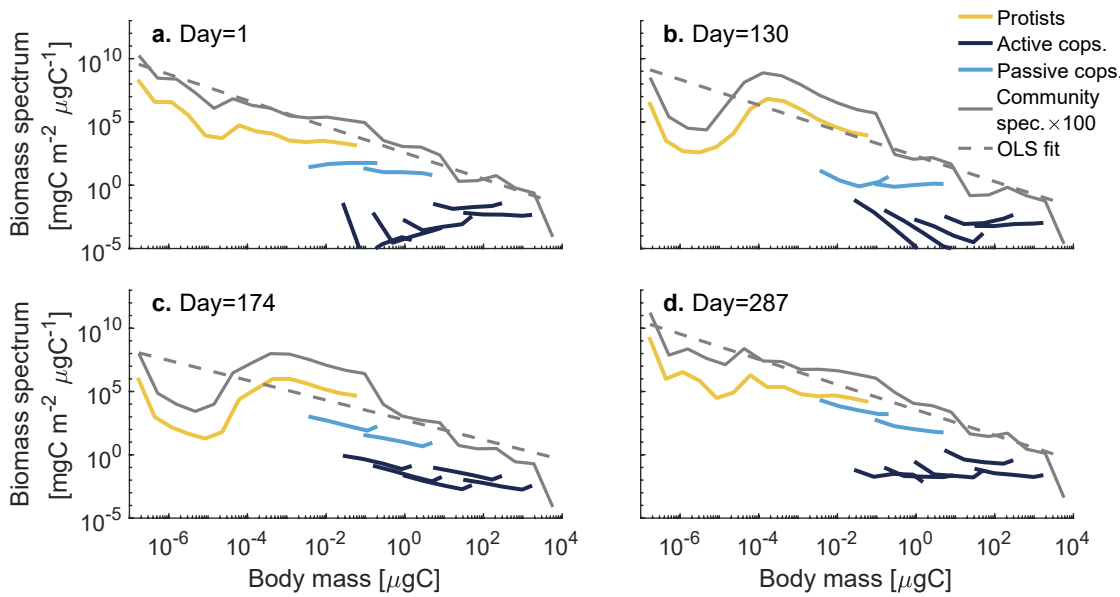

Figure 6. Normalized biomass spectra of the community at different times of the year in the North Atlantic: (a) winter, (b) spring, (c) summer, (d) autumn. Protists (yellow), active copepods (dark blue), passive copepods (light blue). Biomass spectra of the community (gray, we multiplied it by 100 for better visualisation), and least squares fit (gray dashed line). To calculate the community spectrum, the community was divided into 24 logarithmic evenly distributed mass groups, and therefore the resolution is coarser than the spectrum within each group. The community spectrum does not include detritus.

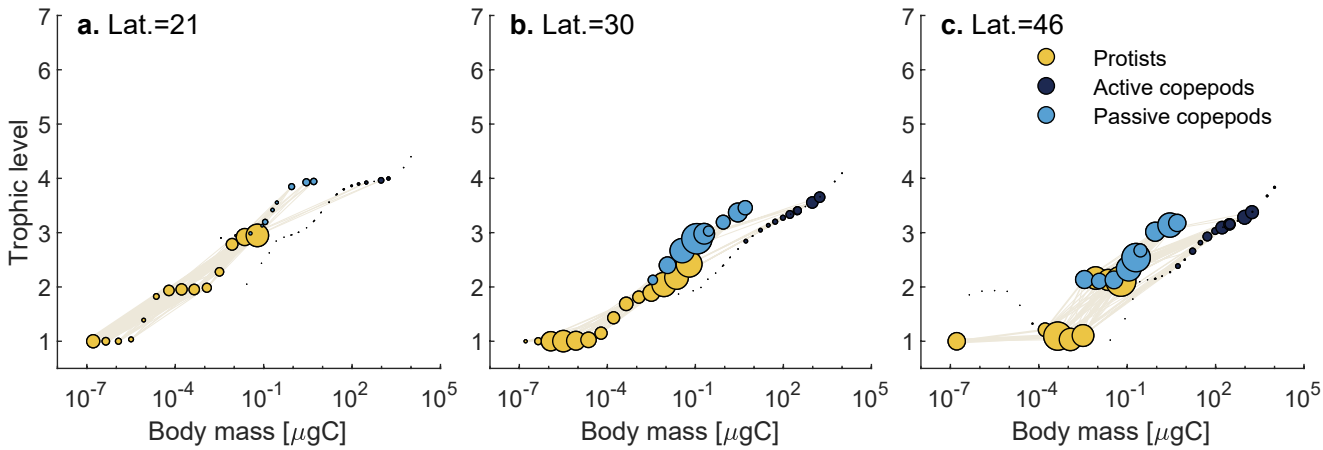

Figure 7. Food-webs emerging from the model shown as trophic levels (*y*-axis) versus body-mass (*x*-axis) for three latitudes (21, 30, 46, specific locations in Figure D9 in Supporting Information S1) in the North Pacific. Circle size (area) represents biomass relative to a common value for all panels. Lines connecting circles show the strength of the trophic interaction (i.e., predation, smallest values have been removed for clarity). Trophic level is calculated as explained in Supporting Information S1 section b. Decimal trophic levels can occur due to a correction to account for mixotrophy. This also results in some large protists having a lower trophic level than their prey.

3.3. Food-Web Structure and Trophic Level

Food-web structure and trophic levels vary across regions and time (Figures 2c and 7). The average trophic level of active copepods is highest in oligotrophic regions (Figure 2c), where it is close to level 4, indicating long food-webs. The biomass of active copepods in these oligotrophic regions is fairly low. In temperate and sub-arctic regions, the average trophic level of active copepods decreases to between 2 and 3 (Figures 2c and 7). This occurs when the size of primary producers increases (e.g., Figures 7b and 7c versus a). Trophic levels close to two indicate that copepods feed mostly on primary producers, efficiently transferring energy to large organisms that produce fast-sinking particles.

Copepods of different sizes can have similar trophic levels (Figures 7b and 7c). Small passive copepods often have the same trophic level as large active copepods. This is due to the lower predator-prey mass ratio of passive feeding copepods relative to active feeders. Hence, communities dominated by passive feeders are less efficient than communities dominated by active feeders at transferring energy to large organisms and exporting carbon.

3.4. Primary Production, Carbon Flux and Export Efficiency

Yearly averaged NPP is high in temperate and equatorial regions and lowest in the oligotrophic gyres (Figure 8a). The annual global NPP is 65 PgC year^{-1}, falling within the range of global NPP estimated by remote sensing (between 36 and 78 PgC year^{-1}, Carr et al., 2006). Compared to field data (Figure 9a), our model performs well in some regions such as the North Atlantic and BATS but does not perform well in the Southern Ocean, where it can underestimate NPP by more than an order of magnitude in some areas. This may be due to the coarse resolution of our physical model, which results in low light levels in the surface layers. Also, NPP values in the Southern Ocean are large and variable, possibly due to some of the data being collected in a frontal zone and close to the coast, which are not well resolved by the transport matrix. Still, the RMSD values in most regions are similar to, or lower than, the ones obtained from other NPP models (Saba et al., 2011), including remote sensing ones (note that the comparison might sometimes be imprecise due to data averaging in some bins of the transport matrix).

Global carbon export is 7.2 PgC year^{-1} at 120 m (and 0.98 PgC year^{-1} at 1,080 m), which is within recent estimates of global carbon export (6.6 PgC year^{-1} in Siegel et al. (2014) and 9.1 PgC year^{-1} in DeVries and Weber (2017)). Yearly integrated carbon export is highest in tropical and in temperate regions (Figures 8b and 8c). Compared to field data of ^{234}Th (Figure 9b), the spread is large and the model tends to overestimate the export flux. Compared

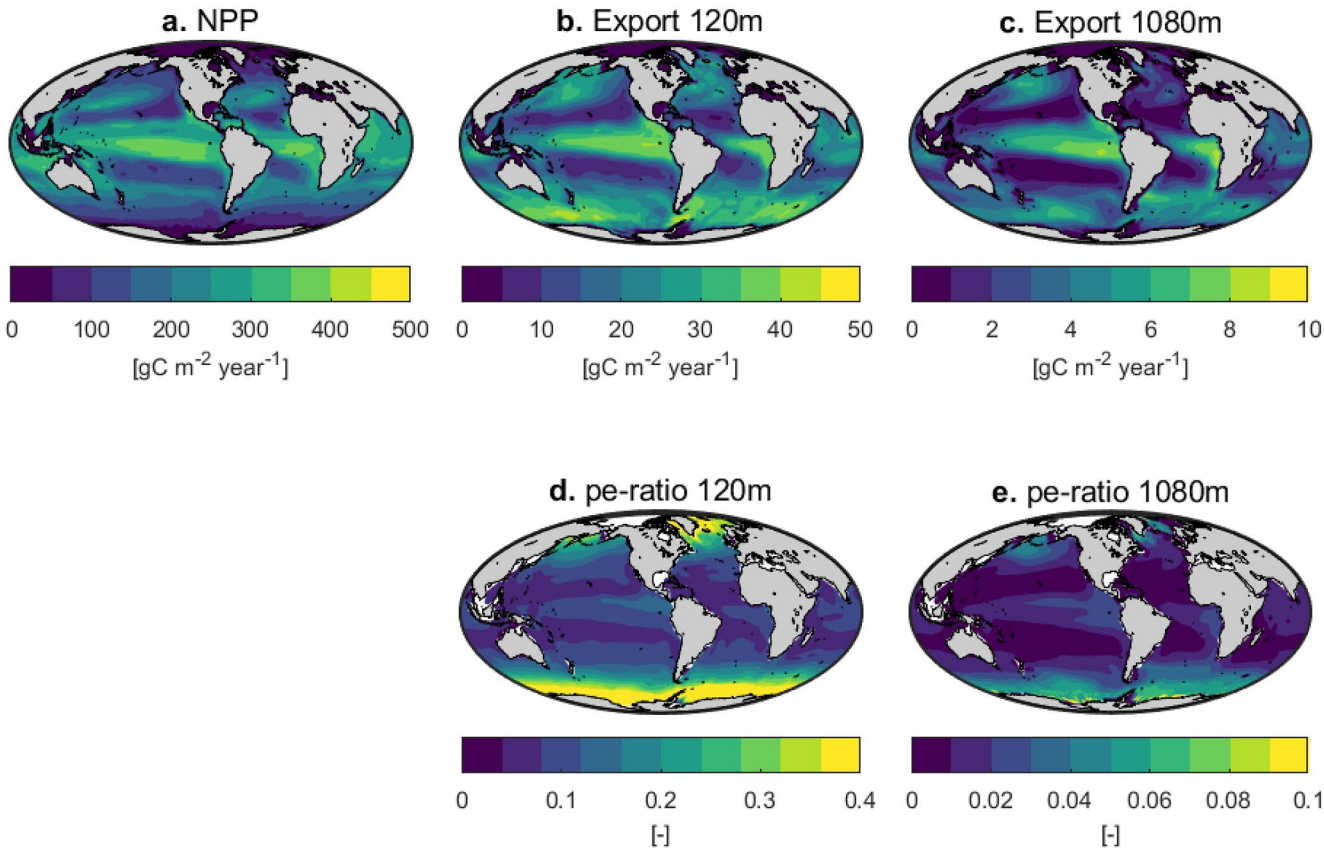

Figure 8. Yearly integrated (a) Net primary production, (b) particle export at 120 m, (c) particle export at 1,080 m, (d) pe-ratio at 120 m, (e) pe-ratio at 1,080 m.

to sediment traps, the model underestimates deep export (Figure 9c), but overall the profiles fall within observed ranges (Figures 9d–9g).

The yearly pe-ratio at 120 m ranges between ≈0 in oligotrophic regions to more than 0.4 in polar regions, and pe-ratio at 1,080 m is below 0.08 in most regions (Figures 8d and 8e).

The composition of the sinking material varies across regions and depth (Figure 10). Deadfalls dominate export at 120 m in most regions, particularly in oligotrophic regions, in the North Atlantic, and in the Southern Ocean (Figure 10a). Elsewhere, fecal pellets have a combined contribution close to one third of the export flux (Figures 10b and 10c). However, deep export (1,080 m), is dominated by fecal pellets produced by large copepods (Figure 10f), except in the Southern Ocean, oligotrophic regions and the North Atlantic. In these regions, dead cells still contribute about 60% of the deep export (Figure 10d). In conclusion, the composition of the carbon export is highly variable close to the surface, but is mainly dominated by large fecal pellets below 1,000 m.

3.5. Relation Between Export, Pe-Ratio and Community Metrics

To explore the relations between community metrics and carbon export, we performed a correlation analysis of export and pe-ratio at 120 and 1,080 m with the exponent of the size spectrum, the average trophic level of active copepods, and copepod biomass (Figure 11). We also compared the performance of these community metrics with other more commonly used metrics such as NPP and sea surface temperature (SST). We use the Spearman correlation coefficient (ρ) to quantify the correlation strength.

The exponent of the size spectrum is the variable that has the strongest correlation with surface and deep pe-ratio ($\rho = 0.87$ and $\rho = 0.94$ respectively, Figures 11k and 11p). Large exponents ("flatter" spectra) result in high and efficient export, whereas low exponents (steeper spectra) result in low and inefficient export. That is because

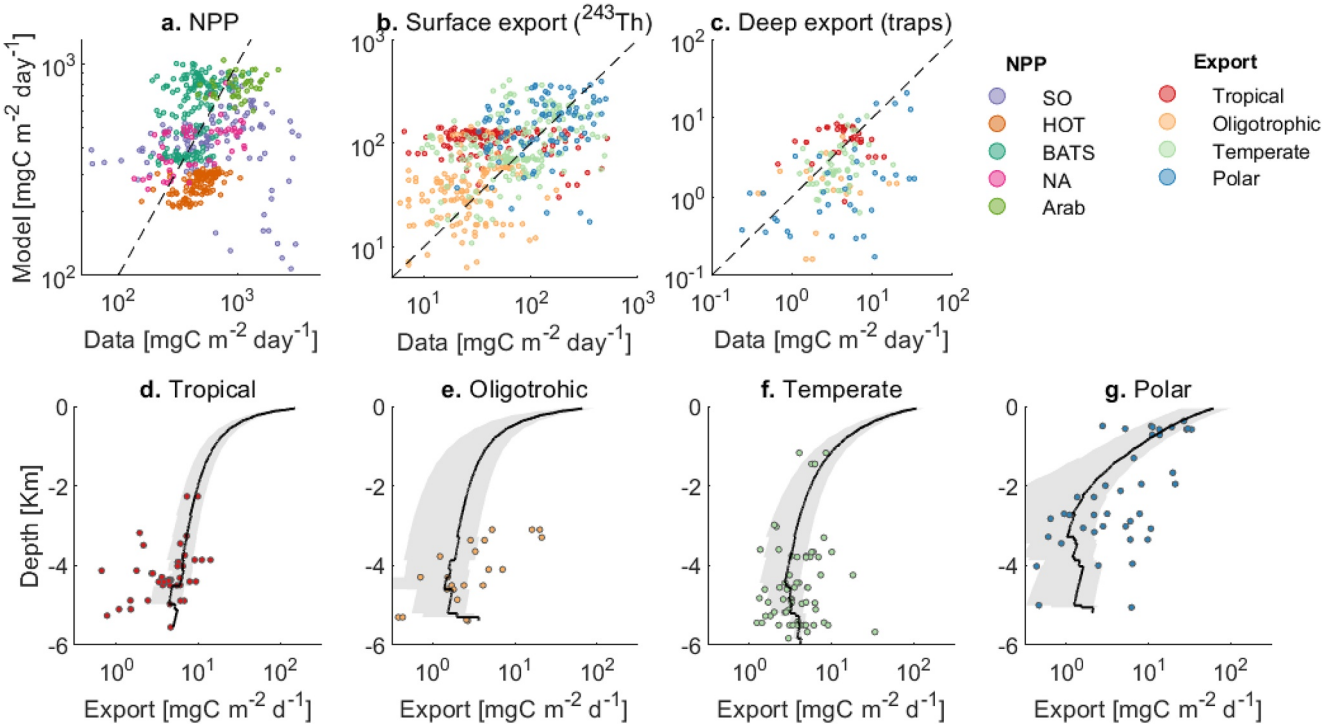

Figure 9. Model versus data of (a) Net primary production and (b) carbon export obtained from the ^{234}Th technique (depth ranging 54–231 m) and (c)–(g) from sediment traps (depth ranging 365–6,100 m). Colors in panel a show different ocean regions: Southern Ocean (SO, root mean square difference (RMSD) = 0.55), Hawaii Ocean Time-series (HOT, RMSD = 0.04), Bermuda Atlantic Time-series Study (BATS, RMSD = 0.14), eastern North Atlantic (NA, RMSD = 0.09), and Arabian Sea (Arab, RMSD = 0.05). For visualization purposes the *y*-axis in this panel have been limited, and some data points corresponding to the southern ocean that the model underestimates are not shown (the full figure can be seen in the Supporting Information S1, Figure D7). Colors in panel b–g show different biomes obtained by grouping Longhurst regions and excluding coastal areas (Figure D6 in the Supporting Information S1): Tropical ($RMSD_{Th}$ = 0.13, $RMSD_{Traps}$ = 0.28), oligotrophic ($RMSD_{Th}$ = 0.34, $RMSD_{Traps}$ = 0.47), temperate ($RMSD_{Th}$ = 0.39, $RMSD_{Traps}$ = 0.22) and polar ($RMSD_{Th}$ = 0.33, $RMSD_{Traps}$ = 0.53). Depth profiles show the sediment trap data (dots) and the average profile (black line) and standard deviation (gray shading) of the model in all the sampled sites for each region. NPP data was obtained from the data set compiled in Saba et al. (2011), carbon export data using the ^{234}Th technique from the data set compiled in Le Moigne et al. (2013) and extended in Henson et al. (2019), and carbon export data from sediment traps from the data set in (Lutz et al., 2007). Data that fell within the same day and bin of the transport matrix has been averaged. See Figures D4 and D5 in the Supporting Information S1 for sampling locations.

the exponent of the size spectrum provides information on how efficiently energy reaches large organisms that are efficient carbon exporters.

Copepod biomass correlates well with carbon export (ρ = 0.70 at surface and ρ = 0.80 at depth, Figures 11b and 11g). This is not surprising, since in the model, copepods produce faster-sinking particles relative to protists. Due to the relative constant size-distribution of copepods, an increase in copepod biomass also incurs an increase in large copepods that contribute the most to deep export. On the other hand, surface pe-ratio is not linearly related to copepod biomass (ρ = 0.48, Figure 11l). In this case, there is a lower bound of copepod biomass until which pe-ratio and copepod biomass are uncorrelated, and after this threshold is surpassed, any kind of pe-ratio can be found. This effect is smoothed for the deep pe-ratio, where the correlation coefficient increases (ρ = 0.74, Figure 11q).

The average trophic level of active copepods has the strongest correlation with carbon export both at surface and depth (ρ = −0.84 and ρ = −0.81 respectively, Figures 11c and 11h). The correlation is negative, implying that the higher the trophic level (i.e., the larger the food-web), the lower the carbon export and export efficiency. This suggests that more carbon is respired in the surface ocean instead of being exported.

NPP shows two trends with carbon export (Figures 11d and 11i), one for low latitudes and another for high latitudes. NPP correlates negatively with pe-ratio at higher latitudes and has no clear relation at low latitudes (Figure 11n). The scatter is large and correlation coefficients tend to be somewhat low, showing that using NPP to estimate export and pe-ratio in all regions might not be the best method. However, using different algorithms

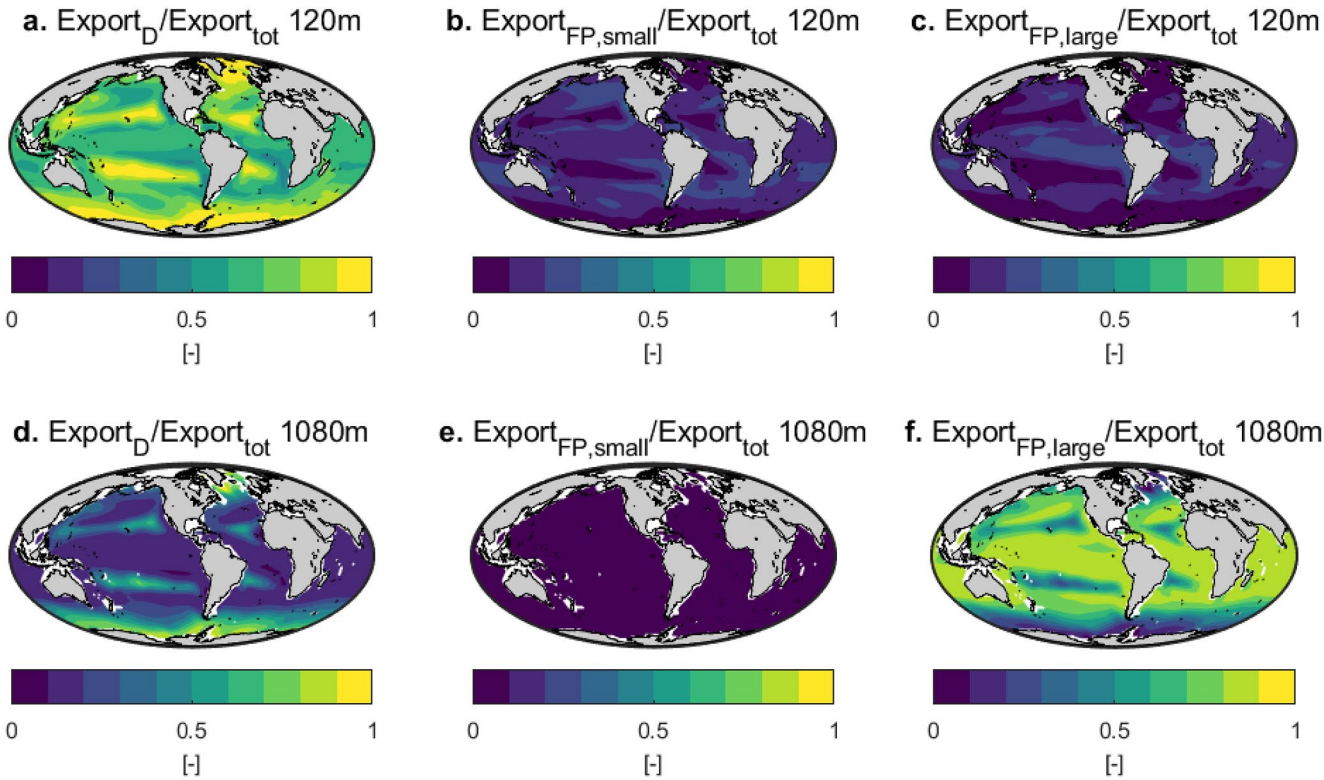

Figure 10. Contribution to total export from dead cells (a),(d), fecal pellets from small copepods (b),(e), and from large copepods (c),(f) at 120 m (upper panels) and 1,080 m (lower panels). Small copepods are below 1 mm.

for specific regions might improve the fit, since, in the model, trends with carbon export seem to be more clear at low latitudes (Figures 11d and 11i).

Finally, temperature shows no clear relation with export ($\rho = -0.42$ at surface and $\rho = -0.28$ at depth, Figures 11e and 11j), but is strongly related to pe-ratio at surface ($\rho = -0.81$ Figure 11o), even thought this effect is weakened for deep pe-ratio ($\rho = -0.65$ Figure 11t).

Overall, at the annual level, carbon export correlates best with total copepod biomass and the average trophic level of active copepods. pe-ratio at surface correlates best with the exponent of the size spectrum and with temperature, even though pe-ratio at depth correlates particularly well with the exponent of the size spectrum. Finally, NPP did not show any clear trend with either export or pe-ratio. Overall, plankton community metrics were better correlated with deep export and deep pe-ratio than NPP or SST were.

3.6. Seasonality and Time-Lags

Until now we have considered yearly integrated rates. However, the dynamics of export and its efficiency vary over the season. We examine this in three regions with different dynamics: North Pacific, North Atlantic and an oligotrophic gyre. The North Pacific has large copepods throughout the year (Figure 12d) and a gradual increase of phytoplankton biomass and NPP during spring (Figure 12g). The North Atlantic has a spring peak in NPP (reflecting a phytoplankton bloom) almost twice as intense as in the North Pacific (Figure 12h) and copepods appear relatively late in the season (Figure 12e). Finally, the oligotrophic gyre has a very low copepod biomass and is dominated by a microbial food-web (Figures 12c and 12f).

The different dynamics between the North Atlantic and North Pacific emerge from the differences in winter phytoplankton biomass due to deep mixing. In the North Pacific, copepods are sustained by protists biomass during the winter, and are able to control the phytoplankton spring bloom, which is therefore not very pronounced. There is still a time-lag between copepods and protists, but shorter compared to the one in the North Atlantic.

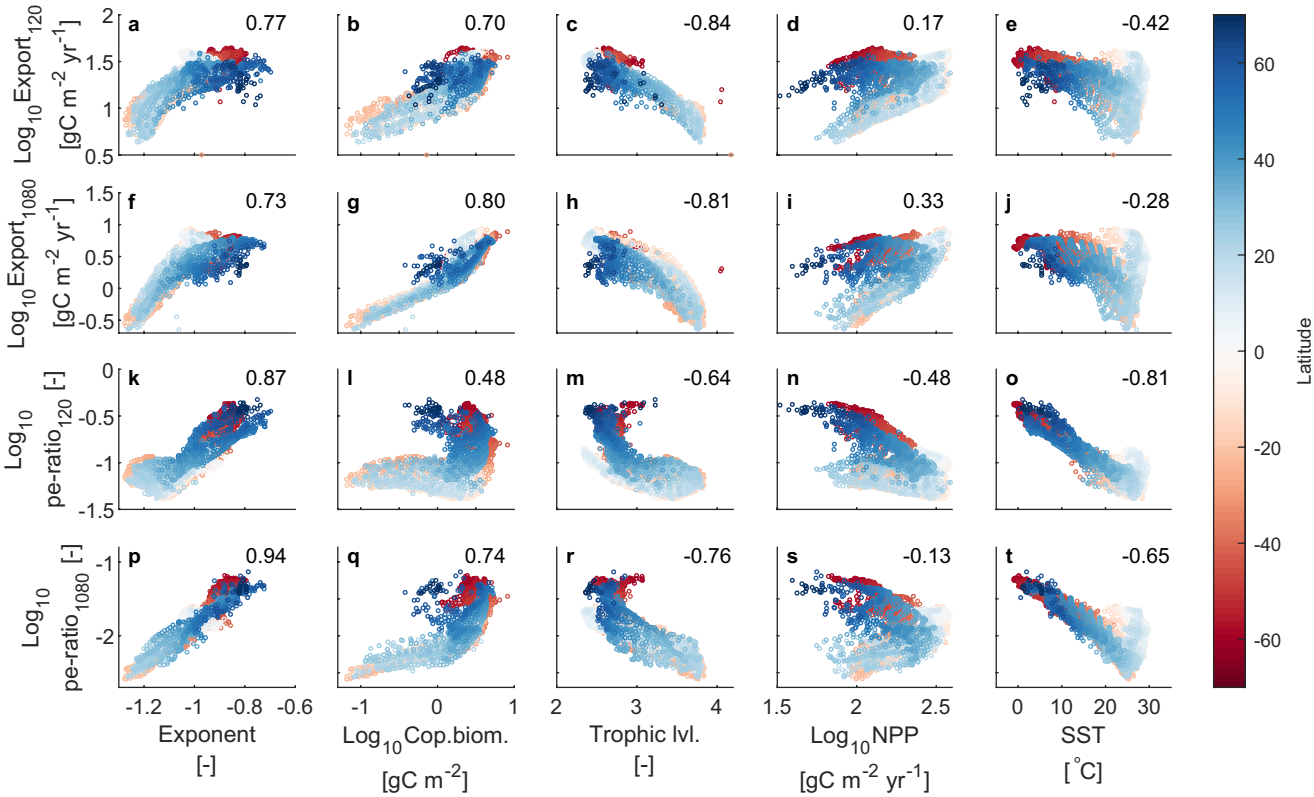

Figure 11. Correlation plots for export and pe-ratio at 120 and 1,080 m against the exponent of the size-spectrum (a,f,k,p), copepod biomass (b,g,l,q), average trophic level of active copepods (c,h,m,r), Net primary production (d,i,n,s), and sea surface temperature (e,j,o,t). Rates are yearly integrated, the rest is yearly averaged. Numbers in the upper corner of each panel show the Spearman correlation coefficient ρ (we use Spearman ρ since some variables are not linearly related).

Here, pe-ratio at depth is fairly high during the whole year due to the large copepod biomass, in contrast to the North Atlantic.

In the north Atlantic, copepod biomass is lower because copepods need to recover from the deep winter mixing. The delay between the spring bloom and peak biomass is also longer, and therefore most export is dominated by dead protists in spring during and after the bloom (Figure 12k). In this case, the pe-ratio at 120 m is very high just after the bloom, but is heavily attenuated due to the slower sinking rates and therefore does not result in a high pe-ratio at 1,000 m. Hence, time-lags affect the composition of the export flux, but not necessarily the pe-ratio. Ultimately the pe-ratio is defined by total export, the fast dynamics of NPP relative to export (e.g., after the bloom), and community composition, the latter defining the sinking rates of particles.

The exponent of the size spectrum follows surface pe-ratio time trends, but does not necessarily follow the trend of deep pe-ratio (Figures 12p–12u). It thus seems that pe-ratio correlates well with variation of the exponent across regions but not necessarily over time within a specific region.

4. Discussion

We sought to understand how carbon export and its efficiency relate to the size spectrum and community composition of the planktonic community. These metrics included the exponent of the size spectrum, trophic level of organisms, and copepod biomass. We also wanted to understand how time-lags between primary producers and copepods affected export and its efficiency. The analysis was made with a mechanistic trait-based model that resolves the size structure of both the planktonic community and the sinking detritus. Food web structures and size spectra emerge from the model rather than being prescribed. Simulated biomass of copepods and protists follow well observed trends from field data. The emergent food-webs and size-spectra result in differences in carbon export and its efficiency.

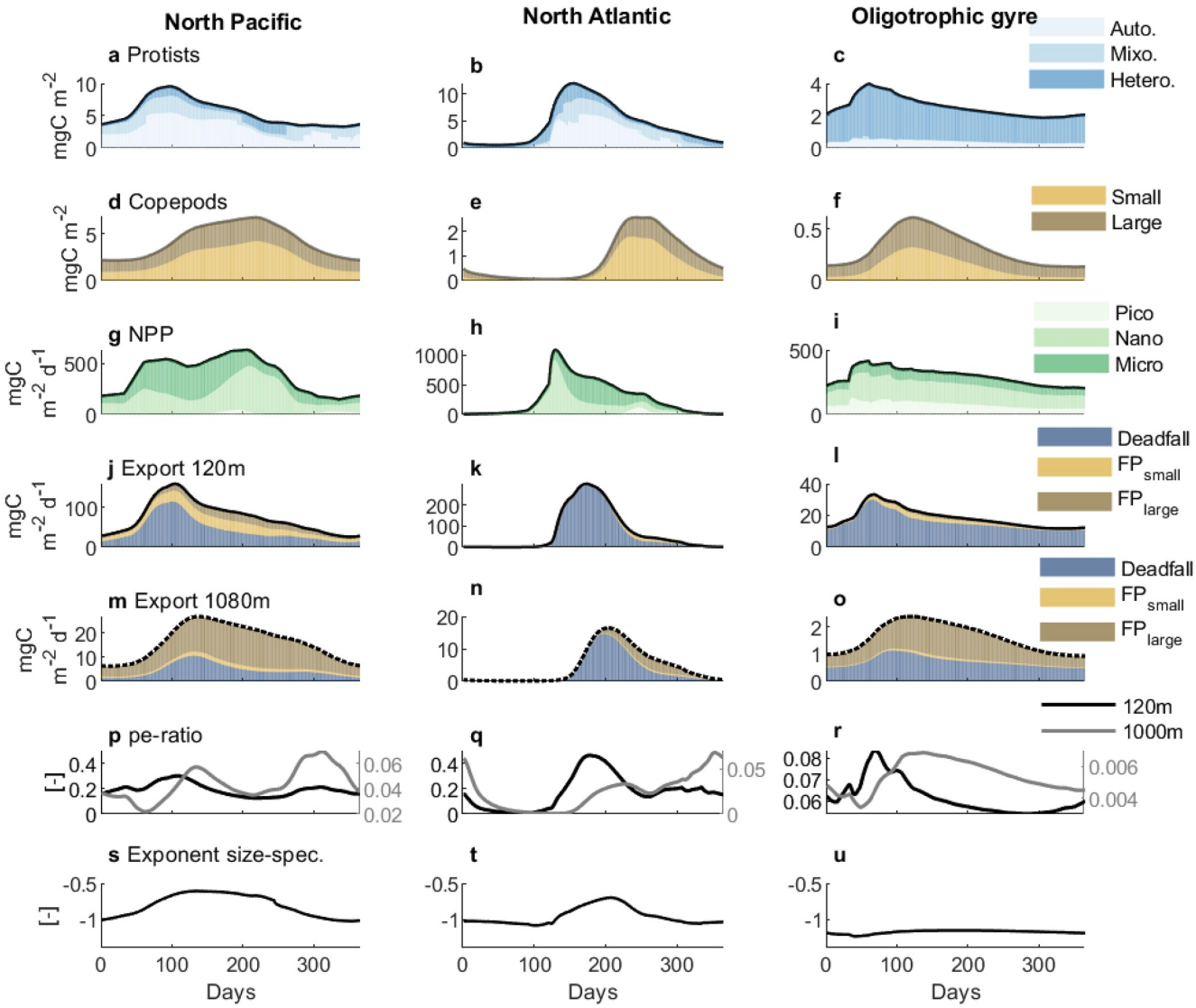

Figure 12. Seasonal dynamics in the North Pacific, North Atlantic and an oligotrophic region (a,b,c) biomass of protists (d,e,f) biomass of copepods (g,h,i) net primary production (j–o) export at 120 m and at 1,080 m (p–r) pe-ratio at 120 and 1,080 m and (s–u) exponent of the normalized size spectrum. Note different scales on the *y*-axis within columns. Specific locations in Figure D9 in Supporting Information S1.

The main results are: (a) carbon export correlates best with copepod biomass and the average trophic level of active copepods, whereas (b) pe-ratio correlates best with the exponent of the size spectrum and SST. (c) These community metrics correlate better with deep export and deep pe-ratio than commonly used metrics, such as NPP or SST. Finally, (d) time-lags between phytoplankton and copepods change the composition of the material exported, but do not strongly affect export or pe-ratio at depth.

4.1. Can We Use Size Spectra to Estimate Carbon Export and Its Efficiency?

An interesting avenue could be to use the parameters of the size spectrum to estimate export fluxes. However, measuring a size spectrum in the field is demanding, as it requires sampling organisms/particles that range several orders of magnitude in mass. Hence, many studies focus on sampling only one part of the size spectrum (e.g., phytoplankton). Dynamics of specific size-groups of unicellular organisms can quickly vary in time, for example, during a phytoplankton bloom. In such conditions, a power-law will not fit the spectrum when only the phytoplankton size-range is considered (Figures 6b and 6c and Figures D1, D2 and D3 in the Supporting Information S1). The irregularities observed in size spectra (often referred as "domes") are common (Sheldon

& Parsons, 1967). These domes reflect other properties of the food-web, such as changing top-versus bottom-up control within a size range (Rossberg et al., 2019). In a meta-analysis, it has also been shown that to represent energy transfer faithfully, size spectra need to span more than seven orders of magnitude in carbon mass (Atkinson et al., 2021).

Field-sampling over a large size range is possible (Atkinson et al., 2021; Lombard et al., 2019), but the space and time resolution of these measurements is scarce and the collection demanding. An approach that would overcome this limitation is to get proxies of the size spectrum via remote sensing (Kostadinov et al., 2009), however this approach still needs to be validated. If sampling plankton size spectra in the field becomes easier to achieve, or if good proxies of the size spectrum are developed, size spectra may become a powerful tool to quantify ecosystem processes such as trophic transfer efficiency to large organisms (such as fish) and carbon export to the deep ocean.

4.2. Export, Pe-Ratio, and Time-Lags

Time-lags between primary production and peak copepod biomass do not affect carbon export or its efficiency *per-se*. They mainly affect the composition of the material being exported. Some studies suggest that strong trophic coupling between phytoplankton and their predators can reduce export and its efficiency due to trophic transfer losses and higher remineralization rates in the surface ocean (Henson et al., 2019; Parsons, 1988). These studies often assume the predator to be mesozooplankton. However, here, we show that deep export is maximal when copepod biomass is high. Conversely, dominance by protists during spring blooms results in large surface export, but not deep export. We expect this latter result to change if formation of detrital aggregates was modeled. As aggregates become larger, their sinking rates increase. This may particularly happen during diatom blooms, potentially resulting in a high export and pe-ratio in "uncoupled systems". Overall, whether export and its efficiency are high or low in coupled or uncoupled systems depend on how efficient prey are at exporting carbon relative to their predators.

Another result from the model is that surface export often lags NPP, and deep export does not follow NPP dynamics. These differences in timing between export and NPP complicates the interpretation of pe-ratio values. For instance, the pe-ratio at surface follows carbon export, whereas the deep pe-ratio is not necessarily higher when deep export is high. Rather, the deep pe-ratio increases when NPP decreases. These differences in rate of change of export end NPP have been shown to give different pe-ratios depending on how NPP is averaged (Laws & Maiti, 2019). Total export has a more intuitive dynamic than pe-ratio, since pe-ratio is a function of two rates that vary at different time-scales and where the uncertainties of both measurements are propagated. Thus, estimating total export may be more useful than attempting to estimate the pe-ratio from NPP.

4.3. Contribution by Copepods to Carbon Export

Deep export in most regions is dominated by fecal pellets of large copepods. This result agrees with other studies that found copepod size to be an important driver of carbon export (Stamieszkin et al., 2015). This is, however, not necessarily supported by other studies. Using field data, a recent study found regimes of low carbon export in regions where macrozooplankton biomass and bacteria were high (Henson et al., 2019). Other studies argue that copepods can strongly attenuate the carbon flux by fragmenting detrital particles (Cavan et al., 2017; Mayor et al., 2020; Wexels Riser et al., 2007, 2010). We consider consumption of detritus by copepods, but not a reduction in particle size due to particle fragmentation. Therefore, in the model, losses by simple trophic transfer are not enough to attenuate the flux.

4.4. Comparison With Other Models and Model Limitations

Our model fits biomass data relatively well, but less so in terms of NPP and carbon export. Other models which are optimized with observations perform better at estimating these rates (DeVries & Weber, 2017; Siegel et al., 2014; Stock et al., 2014), but provide less mechanistic detail. Still, in terms of NPP, the variation found for each region is lower or similar to the values found in 21 NPP models (Saba et al., 2011). In another model intercomparison, the correlation coefficient between the models and NPP varied from −0.08 to 0.64 (Kwiatkowski et al., 2014). This shows the difficulty to successfully capture biological processes in models, particularly when the model is not optimized to empirical observations.

Our global estimate of carbon export at 120 m, 7.2 PgC year^{-1}, falls within the range of estimated values of some of the most recent studies (6.6 PgC year^{-1} in Siegel et al. (2014) and 9.1 PgC year^{-1} in DeVries and Weber (2017)). However, when comparing carbon export measured in the field, our model tends to overestimate export close to the surface and underestimate it in the deeper layer. On one hand, this might be due to the surface export data that we have used, where export was estimated with the ^{234}Th method (Le Moigne et al., 2013). This approach has been shown to underestimate the carbon flux by approximately 2-fold in some regions (Buesseler et al., 2000; Quay, 1997), due to adsorption of ^{234}Th on filters and preferential collection of suspended versus sinking particles. On the other hand, we might also miss other processes that affect particles sinking rate such as coagulation/fragmentation, porosity, mineral ballast, among other things (Bach et al., 2019). It is clear that more work is needed in this direction, specially considering that carbon export in our model was fairly sensitive to the sinking rate of deadfalls (see sensitivity analysis in section E of the Supporting Information S1). However, the consideration of a size-spectrum of detrital particles, including fecal pellets, and associated sinking rate size-scaling, is seldom included in global models, which tend to model export by using two or three detrital groups (e.g., Henson et al., 2015; Siegel et al., 2014). Even though the formulation of sinking speed with respect to size is uncertain, we think that our assumptions (based on empirical observations) of particle sinking speed with size, specially for fecal pellets, are reasonable and a good starting point to model carbon export.

Despite the high ecological complexity of our model, the biogeochemistry is simplistic. We use nitrogen as the sole nutrient in the system, whereas most global models consider other limiting nutrients such as iron, phosphorus or silica (DeVries & Weber, 2017; Henson et al., 2011; Ward et al., 2018), which can be important limiting factors in some ocean regions. In addition, the coarse resolution of the transport matrix prevented us from obtaining carbon export just below the photic layer, which has been recommended in recent studies (Buesseler et al., 2020). Instead we measured it at fixed depths (120 and 1,080 m) probably causing some biases when comparing carbon export across regions.

Protists in the model are not separated into functional groups. Instead, the trophic strategy (autotrophy, mixotrophy or heterotrophy) emerges as a function of cell size and the environment. This configuration still captures the main dynamics observed in nature: a dominance of small primary producers in oligotrophic regions, larger primary producers in more productive regions, and the constant presence of unicellular zooplankton and the microbial food-web. This simplification becomes an advantage as it captures complex dynamics while being based on a relatively low set of parameters and processes.

Other organisms that may contribute significantly to carbon export but are not included in our model are gelatinous zooplankton (Luo et al., 2020). The inclusion of these organisms would probably increase export due to their large bodies that can quickly sink to the bottom, and their large predator-prey mass ratio. Large predator-prey mass ratios generate "shortcuts" in the food-web, where energy from very small organisms is efficiently transferred to larger ones, further enhancing carbon export and its efficiency. Some recent global models now include gelatinous zooplankton (Heneghan et al., 2020; Wright et al., 2021), but these organisms still lack in most global biogeochemical models.

Finally, we do not represent diel and seasonal vertical migrations of zooplankton. Vertical migration play an important role in the survival and life cycle of copepods, and in carbon export (Hansen & Visser, 2016; Jónasdóttir et al., 2015; Pinti et al., 2021; Steinberg & Landry, 2017). Implementing vertical migrations may be done through optimisation (e.g., Brun et al., 2019; Pinti & Visser, 2019; Pinti et al., 2019). However, implementing behavior together with population dynamics is challenging, especially if considered at the global scale. Implementing the active export pathway is urgently needed, since other modeling studies have suggested that the active carbon flux may have been responsible for increasing the efficiency of the biological carbon pump (Fakhraee et al., 2020).

5. Conclusion

We have investigated how carbon export and its efficiency relate to the size spectrum and community composition of the planktonic community. We have shown that carbon export correlates well with copepod biomass and trophic level, and that pe-ratio correlates best with the exponent of the size spectrum and temperature. Community metrics correlate better with deep export and deep pe-ratio than SST and NPP. Time-lags between phytoplankton and zooplankton do not necessarily affect carbon export or its efficiency. Our framework captures complex

community dynamics scaled from simple individual-level processes. This study has shown the potential of more complex ecological models to explore and understand ecosystem functions and biogeochemical processes at the global scale.

Data Availability Statement

Data-sets for this research are included in these papers (and their supplementary information files): San Martin et al. (2006); Lutz et al. (2007); López and Anadón (2008); Saba et al. (2011); Le Moigne et al. (2013); Henson et al. (2019). The MATLAB files of the model can be found in the GitHub repository https://github.com/cam-sp/NUMmodel_global.

Acknowledgments
This work was supported by the Gordon and Betty Moore Foundation through award 5479, and by the Centre for Ocean Life, a VKR Centre for Excellence funded by the Villum Foundation. CSP was also supported by a grant from the Simons Foundation (#722859). B.A.W. was funded by a Royal Society University Research Fellowship.

References

Alldredge, A. L., & Gotschalk, C. (1988). In situ settling behavior of marine snow 1. *Limnology & Oceanography*, *33*(3), 339–351. https://doi.org/10.4319/lo.1988.33.3.0339

Andersen, K. H. (2019). *Fish ecology, evolution, and exploitation: A new theoretical synthesis*. Princeton University Press (ISBN: 0691192952, 9780691192956).

Andersen, K. H., Berge, T., Gonçalves, R. J., Hartvig, M., Heuschele, J., Hylander, S., et al. (2016). Characteristic sizes of life in the oceans, from bacteria to whales. *Annual Review of Marine Science*, *8*(1), 217–241. https://doi.org/10.1146/annurev-marine-122414-034144

Andersen, K. H., Beyer, J., & Lundberg, P. (2009). Trophic and individual efficiencies of size-structured communities. *Proceedings of the Royal Society B: Biological Sciences*, *276*(1654), 109–114. https://doi.org/10.1098/rspb.2008.0951

Andersen, K. H., & Beyer, J. E. (2006). Asymptotic size determines species abundance in the marine size spectrum. *The American Naturalist*, *168*(1), 54–61. https://doi.org/10.1086/504849

Atkinson, A., Lilley, M. K., Hirst, A. G., McEvoy, A. J., Tarran, G. A., Widdicombe, C., et al. (2021). Increasing nutrient stress reduces the efficiency of energy transfer through planktonic size spectra. *Limnology & Oceanography*, *66*(2), 422–437. https://doi.org/10.1002/lno.11613

Bach, L. T., Stange, P., Taucher, J., Achterberg, E. P., Algueró-Muñiz, M., Horn, H., et al. (2019). The influence of plankton community structure on sinking velocity and remineralization rate of marine aggregates. *Global Biogeochemical Cycles*, *33*(8), 971–994. https://doi.org/10.1029/2019GB006256

Bisson, K., Siegel, D. A., & DeVries, T. (2020). Diagnosing mechanisms of ocean carbon export in a satellite-based food web model. *Frontiers in Marine Science*, *7*. https://doi.org/10.3389/fmars.2020.00505

Brun, P., Stamieszkin, K., Visser, A. W., Licandro, P., Payne, M. R., & Kiørboe, T. (2019). Climate change has altered zooplankton-fuelled carbon export in the north Atlantic. *Nature ecology & evolution*, *3*(3), 416–423. https://doi.org/10.1038/s41559-018-0780-3

Buesseler, K. O., Bacon, M. P., Cochran, J. K., & Livingston, H. D. (1992). Carbon and nitrogen export during the jgofs North Atlantic bloom experiment estimated from 234th: 238u disequilibria. *Deep-Sea Research Part A. Oceanographic Research Papers*, *39*(7–8), 1115–1137. https://doi.org/10.1016/0198-0149(92)90060-7

Buesseler, K. O., Boyd, P. W., Black, E. E., & Siegel, D. A. (2020). Metrics that matter for assessing the ocean biological carbon pump. *Proceedings of the National Academy of Sciences*, *117*(18), 9679–9687. https://doi.org/10.1073/pnas.1918114117

Buesseler, K. O., Steinberg, D. K., Michaels, A. F., Johnson, R. J., Andrews, J. E., Valdes, J. R., & Price, J. F. (2000). A comparison of the quantity and composition of material caught in a neutrally buoyant versus surface-tethered sediment trap. *Deep Sea Research Part I: Oceanographic Research Papers*, *47*(2), 277–294. https://doi.org/10.1016/s0967-0637(99)00056-4

Carr, M.-E., Friedrichs, M. A., Schmeltz, M., Aita, M. N., Antoine, D., Arrigo, K. R., et al. (2006). A comparison of global estimates of marine primary production from ocean color. *Deep Sea Research Part II: Topical Studies in Oceanography*, *53*(5–7), 741–770. https://doi.org/10.1016/j.dsr2.2006.01.028

Cavan, E. L., Henson, S. A., Belcher, A., & Sanders, R. (2017). Role of zooplankton in determining the efficiency of the biological carbon pump. *Biogeosciences*, *14*(1), 177–186. https://doi.org/10.5194/bg-14-177-2017

Chakraborty, S., Nielsen, L. T., & Andersen, K. H. (2017). Trophic strategies of unicellular plankton. *The American Naturalist*, *189*(4), E77–E90. http://orcid.org/0000-0003-4177-3205

DeVries, T., & Weber, T. (2017). The export and fate of organic matter in the ocean: New constraints from combining satellite and oceanographic tracer observations. *Global Biogeochemical Cycles*, *31*(3), 535–555. https://doi.org/10.1002/2016GB005551

Ducklow, H. W., Steinberg, D. K., & Buesseler, K. O. (2001). Upper ocean carbon export and the biological pump. *Oceanography*, *14*(4), 50–58. https://doi.org/10.5670/oceanog.2001.06

Dunne, J. P., Armstrong, R. A., Gnanadesikan, A., & Sarmiento, J. L. (2005). Empirical and mechanistic models for the particle export ratio. *Global Biogeochemical Cycles*, *19*(4). https://doi.org/10.1029/2004GB002390

Dutkiewicz, S., Follows, M. J., & Parekh, P. (2005). Interactions of the iron and phosphorus cycles: A three-dimensional model study. *Global Biogeochemical Cycles*, *19*(1). https://doi.org/10.1029/2004GB002342

Fakhraee, M., Planavsky, N. J., & Reinhard, C. T. (2020). The role of environmental factors in the long-term evolution of the marine biological pump. *Nature Geoscience*, *13*(12), 812–816. https://doi.org/10.1038/s41561-020-00660-6

Hansen, A. N., & Visser, A. W. (2016). Carbon export by vertically migrating zooplankton: An optimal behavior model. *Limnology & Oceanography*, *61*(2), 701–710. https://doi.org/10.1002/lno.10249

Hartvig, M., Andersen, K. H., & Beyer, J. E. (2011). Food web framework for size-structured populations. *Journal of Theoretical Biology*, *272*(1), 113–122. https://doi.org/10.1016/j.jtbi.2010.12.006

Heneghan, R. F., Everett, J. D., Sykes, P., Batten, S. D., Edwards, M., Takahashi, K., et al. (2020). A functional size-spectrum model of the global marine ecosystem that resolves zooplankton composition. *Ecological Modelling*, *435*, 109265. https://doi.org/10.1016/j.ecolmodel.2020.109265

Henson, S., Le Moigne, F., & Giering, S. (2019). Drivers of carbon export efficiency in the global ocean. *Global Biogeochemical Cycles*, *33*(7), 891–903. https://doi.org/10.1029/2018GB006158

Henson, S., Sanders, R., Madsen, E., Morris, P. J., Le Moigne, F., & Quartly, G. D. (2011). A reduced estimate of the strength of the ocean's biological carbon pump. *Geophysical Research Letters*, *38*(4). https://doi.org/10.1029/2011GL046735

Henson, S. A., Yool, A., & Sanders, R. (2015). Variability in efficiency of particulate organic carbon export: A model study. *Global Biogeochemical Cycles*, *29*(1), 33–45. https://doi.org/10.1002/2014gb004965

Jónasdóttir, S. H., Visser, A. W., Richardson, K., & Heath, M. R. (2015). Seasonal copepod lipid pump promotes carbon sequestration in the deep north Atlantic. *Proceedings of the National Academy of Sciences*, *112*(39), 12122–12126. https://doi.org/10.1073/pnas.1512110112

Khatiwala, S. (2007). A computational framework for simulation of biogeochemical tracers in the ocean. *Global Biogeochemical Cycles*, *21*(3). https://doi.org/10.1029/2007GB002923

Khatiwala, S., Visbeck, M., & Cane, M. A. (2005). Accelerated simulation of passive tracers in ocean circulation models. *Ocean Modelling*, *9*(1), 51–69. https://doi.org/10.1016/j.ocemod.2004.04.002

Kiørboe, T., & Hirst, A. G. (2014). Shifts in mass scaling of respiration, feeding, and growth rates across life-form transitions in marine pelagic organisms. *The American Naturalist*, *183*(4), E118–E130. https://doi.org/10.1086/675241

Kostadinov, T., Siegel, D., & Maritorena, S. (2009). Retrieval of the particle size distribution from satellite ocean color observations. *Journal of Geophysical Research*, *114*(C9), C09015. https://doi.org/10.1029/2009jc005303

Kwiatkowski, L., Yool, A., Allen, J., Anderson, T., Barciela, R., Buitenhuis, E., et al. (2014). Imarnet: An ocean biogeochemistry model intercomparison project within a common physical ocean modelling framework. *Biogeosciences*, *11*(24), 7291–7304. https://doi.org/10.5194/bg-11-7291-2014

Laws, E. A., Falkowski, P. G., Smith, W. O., Jr., Ducklow, H., & McCarthy, J. J. (2000). Temperature effects on export production in the open ocean. *Global Biogeochemical Cycles*, *14*(4), 1231–1246. https://doi.org/10.1029/1999GB001229

Laws, E. A., & Maiti, K. (2019). The relationship between primary production and export production in the ocean: Effects of time lags and temporal variability. *Deep Sea Research Part I: Oceanographic Research Papers*, *148*, 100–107. https://doi.org/10.1016/j.dsr.2019.05.006

Le Moigne, F., Henson, S., Sanders, R., & Madsen, E. (2013). Global database of surface ocean particulate organic carbon export fluxes diagnosed from the 234th technique. *Earth System Science Data*, *5*(2), 295–304. https://doi.org/10.5194/essd-5-295-2013

Lombard, F., Boss, E., Waite, A. M., Vogt, M., Uitz, J., Stemmann, L., et al. (2019). Globally consistent quantitative observations of planktonic ecosystems. *Frontiers in Marine Science*, *6*, 196. https://doi.org/10.3389/fmars.2019.00196

Longhurst, A. R., & Harrison, W. G. (1989). The biological pump: Profiles of plankton production and consumption in the upper ocean. *Progress in Oceanography*, *22*(1), 47–123. https://doi.org/10.1016/0079-6611(89)90010-4

López, E., & Anadón, R. (2008). Copepod communities along an Atlantic meridional transect: Abundance, size structure, and grazing rates. *Deep Sea Research Part I: Oceanographic Research Papers*, *55*(10), 1375–1391. https://doi.org/10.1016/0079-6611(89)90010-4

Luo, J. Y., Condon, R. H., Stock, C. A., Duarte, C. M., Lucas, C. H., Pitt, K. A., & Cowen, R. K. (2020). Gelatinous zooplankton-mediated carbon flows in the global oceans: A data-driven modeling study. *Global Biogeochemical Cycles*, *34*(9), e2020GB006704. https://doi.org/10.1029/2020GB006704

Lutz, M. J., Caldeira, K., Dunbar, R. B., & Behrenfeld, M. J. (2007). Seasonal rhythms of net primary production and particulate organic carbon flux to depth describe the efficiency of biological pump in the global ocean. *Journal of Geophysical Research*, *112*(C10), C10011. https://doi.org/10.1029/2006jc003706

Mayor, D. J., Gentleman, W. C., & Anderson, T. R. (2020). Ocean carbon sequestration: Particle fragmentation by copepods as a significant unrecognised factor? Explicitly representing the role of copepods in biogeochemical models may fundamentally improve understanding of future ocean carbon storage. *BioEssays*, *42*(12), 2000149. https://doi.org/10.1002/bies.202000149

McNair, H. M., Morison, F., Graff, J. R., Rynearson, T. A., & Menden-Deuer, S. (2021). Microzooplankton grazing constrains pathways of carbon export in the subarctic north Pacific. *Limnology & Oceanography*, *66*(7), 2697–2711. https://doi.org/10.1002/lno.11783

Parsons, T. R. (1988). Trophodynamic phasing in theoretical, experimental aud natural pelagic ecosystems. *Journal of the Oceanographical Society of Japan*, *44*(2), 94–101. https://doi.org/10.1007/BF02303124

Pinti, J., Andersen, K. H., & Visser, A. W. (2021). Co-adaptive behavior of interacting populations in a habitat selection game significantly impacts ecosystem functions. *Journal of Theoretical Biology*, *523*, 110663. https://doi.org/10.1016/j.jtbi.2021.110663

Pinti, J., Kiørboe, T., Thygesen, U. H., & Visser, A. W. (2019). Trophic interactions drive the emergence of diel vertical migration patterns: A game-theoretic model of copepod communities. *Proceedings of the Royal Society B*, *286*(1911), 20191645. https://doi.org/10.1098/rspb.2019.1645

Pinti, J., & Visser, A. W. (2019). Predator-prey games in multiple habitats reveal mixed strategies in diel vertical migration. *The American Naturalist*, *193*(3), E65–E77. https://doi.org/10.1086/701041

Quay, P. (1997). Was a carbon balance measured in the equatorial Pacific during jgofs? *Deep Sea Research Part II: Topical Studies in Oceanography*, *44*(9–10), 1765–1781. https://doi.org/10.1016/s0967-0645(97)00093-3

Rossberg, A. G., Gaedke, U., & Kratina, P. (2019). Dome patterns in pelagic size spectra reveal strong trophic cascades. *Nature Communications*, *10*(1), 1–11. https://doi.org/10.1038/s41467-019-12289-0

Saba, V. S., Friedrichs, M. A., Antoine, D., Armstrong, R., Asanuma, I., Behrenfeld, M., et al. (2011). An evaluation of ocean color model estimates of marine primary productivity in coastal and pelagic regions across the globe. *Biogeosciences*, *8*(2), 489–503. https://doi.org/10.5194/bg-8-489-2011

San Martin, E., Harris, R. P., & Irigoien, X. (2006). Latitudinal variation in plankton size spectra in the Atlantic Ocean. *Deep Sea Research Part II: Topical Studies in Oceanography*, *53*(14–16), 1560–1572. https://doi.org/10.1016/j.dsr2.2006.05.006

Serra-Pompei, C., Soudijn, F., Visser, A. W., Kiørboe, T., & Andersen, K. H. (2020). A general size-and trait-based model of plankton communities. *Progress in Oceanography*, *189*, 102473. https://doi.org/10.1016/j.pocean.2020.102473

Sheldon, R., & Parsons, T. (1967). A continuous size spectrum for particulate matter in the sea. *Journal of the Fisheries Board of Canada*, *24*(5), 909–915. https://doi.org/10.1139/f67-081

Siegel, D., Buesseler, K., Doney, S., Sailley, S., Behrenfeld, M. J., & Boyd, P. (2014). Global assessment of ocean carbon export by combining satellite observations and food-web models. *Global Biogeochemical Cycles*, *28*(3), 181–196. https://doi.org/10.1002/2013gb004743

Small, L., Fowler, S., & Ünlü, M. (1979). Sinking rates of natural copepod fecal pellets. *Marine Biology*, *51*(3), 233–241. https://doi.org/10.1007/BF00386803

Sprules, W. G., & Barth, L. E. (2016). Surfing the biomass size spectrum: Some remarks on history, theory, and application. *Canadian Journal of Fisheries and Aquatic Sciences*, *73*(4), 477–495. https://doi.org/10.1139/cjfas-2015-0115

Sprules, W. G., & Munawar, M. (1986). Plankton size spectra in relation to ecosystem productivity, size, and perturbation. *Canadian Journal of Fisheries and Aquatic Sciences*, *43*(9), 1789–1794. https://doi.org/10.1139/f86-222

Stamieszkin, K., Pershing, A. J., Record, N. R., Pilskaln, C. H., Dam, H. G., & Feinberg, L. R. (2015). Size as the master trait in modeled copepod fecal pellet carbon flux. *Limnology & Oceanography*, *60*(6), 2090–2107. https://doi.org/10.1002/lno.10156

Steinberg, D. K., & Landry, M. R. (2017). Zooplankton and the ocean carbon cycle. *Annual Review of Marine Science*, *9*(1), 413–444. https://doi.org/10.1146/annurev-marine-010814-015924

Stock, C., Dunne, J., & John, J. (2014). Drivers of trophic amplification of ocean productivity trends in a changing climate. *Biogeosciences Discussions*, *11*(7), 7125–7135. https://doi.org/10.5194/bg-11-7125-2014

Ward, B. A., Wilson, J. D., Death, R. M., Monteiro, F. M., Yool, A., & Ridgwell, A. (2018). Ecogenie 1.0: Plankton ecology in the cgenie Earth system model. *Geoscientific Model Development*, *11*(10), 4241–4267. https://doi.org/10.5194/gmd-11-4241-2018

Wassmann, P. (1997). Retention versus export food chains: Processes controlling sinking loss from marine pelagic systems. *Hydrobiologia*, *363*(1–3), 29–57. https://doi.org/10.1007/978-94-017-1493-8_3

Wexels Riser, C., Reigstad, M., & Wassmann, P. (2010). Zooplankton-mediated carbon export: A seasonal study in a northern Norwegian fjord. *Marine Biology Research*, *6*(5), 461–471. https://doi.org/10.1080/17451000903437067

Wexels Riser, C., Reigstad, M., Wassmann, P., Arashkevich, E., & Falk-Petersen, S. (2007). Export or retention? Copepod abundance, faecal pellet production and vertical flux in the marginal ice zone through snap shots from the northern Barents Sea. *Polar Biology*, *30*(6), 719–730. https://doi.org/10.1007/s00300-006-0229-z

Wright, R. M., Le Quéré, C., Buitenhuis, E., Pitois, S., & Gibbons, M. J. (2021). Role of jellyfish in the plankton ecosystem revealed using a global ocean biogeochemical model. *Biogeosciences*, *18*(4), 1291–1320. https://doi.org/10.5194/bg-18-1291-2021

References From the Supporting Information

de Roos, A. M., Schellekens, T., Van Kooten, T., Van De Wolfshaar, K., Claessen, D., & Persson, L. (2008). Simplifying a physiologically structured population model to a stage-structured biomass model. *Theoretical Population Biology*, *73*(1), 47–62. https://doi.org/10.1016/j.tpb.2007.09.004

Kiørboe, T. (2000). Colonization of marine snow aggregates by invertebrate zooplankton: Abundance, scaling, and possible role. *Limnology & Oceanography*, *45*(2), 479–484. https://doi.org/10.4319/lo.2000.45.2.0479

Koski, M., Valencia, B., Newstead, R., & Thiele, C. (2020). The missing piece of the upper mesopelagic carbon budget? Biomass, vertical distribution and feeding of aggregate-associated copepods at the pap site. *Progress in Oceanography*, *181*, 102243. https://doi.org/10.1016/j.pocean.2019.102243

Mauchline, J. (1998). The Biology of Calanoid Copepods (Vol. *33*). *Advances in Marine Biology*.

Serra-Pompei, C., Hagstrom, G. I., Visser, A. W., & Andersen, K. H. (2019). Resource limitation determines temperature response of unicellular plankton communities. *Limnology & Oceanography*, *64*(4), 1627–1640. https://doi.org/10.1002/lno.11140

Ward, B. A., & Follows, M. J. (2016). Marine mixotrophy increases trophic transfer efficiency, mean organism size, and vertical carbon flux. *Proceedings of the National Academy of Sciences*, *113*(11), 2958–2963. https://doi.org/10.1073/pnas.1517118113